Design of an Intra-Operative Imaging System for the Cochlear Implant

Calla Klafas[1], Alistair McEwan[1] and Paul Carter[2]

***Abstract*— Research has shown that closer proximity of a cochlear implant electrode array to the inner modiolar wall can improve hearing performance in a recipient. It is understood that developing a real-time intra-operative imaging technique would bring the surgeon visual feedback that can correlate with tactile resistances during electrode insertion, reducing various risks of insertion traumas, while guiding the electrode for optimal placement. This paper presents the design of a 3-dimensional magnetic imaging system which provides a means for real-time imaging by reconstructing uniform segments of the electrode array's contours. In addition, the theoretical error of this reconstruction method is evaluated to select an optimal number of sensors within the electrode design. The theoretical error of the reconstruction method is evaluated for 7 to 22 inductive sensors within the electrode design. For 16 or more sensors, the error is improves to less than 0.5%. A working prototype was confirmed on a 10:1 scale with orthogonal Helmholtz coils at 85-115kHz.**

I. Introduction

It has been determined that cochlear implants perform significantly better in recipients when the placement of the electrode array is located closer to the inner wall of the cochlea corridor, known as the modiolar wall [1]. By stimulating closer to the modiolar wall, a decrease in current spread across targeted neurons allows for finer resolution in pitch perception [2]. More so having closer proximity allows for decreased stimulating thresholds, resulting in reduced power consumption within the implant [3]. It however becomes difficult to insert the electrode at such close proximity, due to the risk of damaging delicate membrane structures of the scala tympani [4].

Visual assistive feedback to a surgeon during an insertion procedure would provide a guide for optimal placement of the electrode while helping to minimize potential trauma. Currently there are no accepted live visualization techniques to assist in inserting the electrode array, since radiographic techniques are non-ideal for younger recipients [5].

Existing research has developed a method for position sensing within a prototype of a MicroElectroMechanical System (MEMS)-based electrode array as part of a future objective to provide sensing feedback for an active position-control mechanism for guided electrode insertion [6]. The electrode array design comprises of an array of eight piezoresistive strain-gauge sensors integrated into a thin-film electrode array. Due to the small helical pitch of the cochlear chamber, the measured changes in resistances due to longitudinal strains are assumed to indicate the average

[1] School of Electrical & Information Engineering, Faculty of Engineering & Information Technologies, The University of Sydney, Australia (phone: 612-9351-8190, fax: 612-9351-3847, e-mail: calla.klafas@sydney.edu.au)

[2] Cochlear Ltd, Sydney, Australia (email: p.carter@cochlear.com)

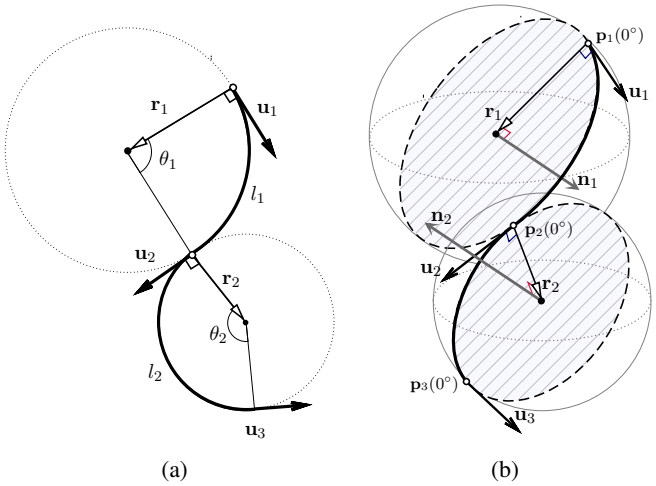

Fig. 1: Graphical representation of the electrode array shape reconstruction in 2D (a) and 3D (b).

2D curvature of each sensor's segments. For the x^{th}, sensor, the geometric shape is recovered by cumulatively combining a piecewise curve of eight assumed uniformly circular arcs, using the average curvature r_x and the known lengths of the segment l_x, while locating the curve to a relative point of origin. With these values, the angle which the arc subtends is calculated by:

$$\theta_x = l_x / r_x \tag{1}$$

Since the strain gauges are only use the longitudinal strains to approximate curvature, the recovery of the electrode array's shape is limited to a 2D plane, orthogonal to the assumed direction of the cochlear helical apex (Fig. 1a).

In this paper we aim to introduce a system which adopts a similar shape-recovery algorithm, but instead recovers the shape of the electrode in 3D. The added value of inspecting the relative position of the array in the direction of the cochlear apex is to detect potential insertion complications, such as basilar membrane perforation [4], not clearly detectable by the assumption of 2D curvature. The similarity in the shape-recovery method is by constructing uniform circular piecewise segments, however each segment is constructed by the tangent vectors of the segments' endpoints. These tangent vectors are acquired by an electrode array design using inductor coils to determine its self-angular orientation relative to the directions of three orthogonal magnetic fields.

Due to the cumulative nature of the shape-recovery algorithm, the position error for the final point of the curve of the sensor array is a summation of the error of each individual segment. At the same time, with an increased number of sensors, the error due to each individual segment decreases,

978-1-4244-7929-0/14/$26.00 ©2014 IEEE

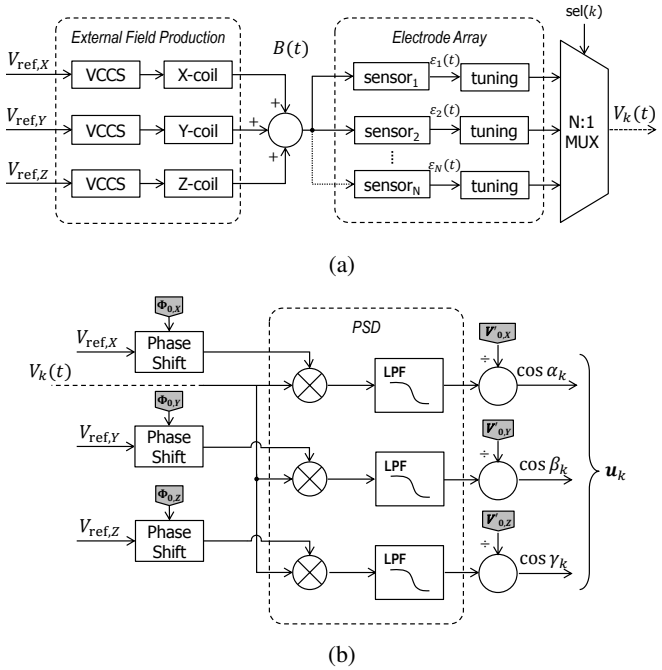

Fig. 2: Block signal diagram of proposed system.

however in such an application, the number of sensors in the electrode array would be limited by manufacturability.

This paper aims to present the design of the 3D magnetic position sensing system and evaluate the shape-recovery algorithm for such an application, where the number of sensing points is limited within the design of the electrode array. This method is analyzed to provide a step forward in proposing an optimal number of sensors and segments for the design of an array within a limit of theoretical accuracy.

II. System Design

This section describes the working principles and design of the intra-operative imaging system. Here the method for shape-recovery is described for a general case where for an array of N tangents, a resultant $N-1$ number of segments are constructed. The tangent vectors are generalized in vector form as $\mathbf{u}_k$ for the k^{th} tangent of the array, while $1 \leq k \leq N$.

These tangent vectors represent the 3D angular orientation of the electrode array's magnetic axial sensors, placed equidistant along the electrode array. In sections II-B & II-C, the working system design used to recover the axial orientations of the sensors is described, which is illustrated and summarised in Fig. 2a & 2b.

A. 3-Dimensional Curve Approximation

As described in section I, a cumulative method of shape recovery for a MEMs-based electrode array is limited to producing a shape in 2D by the technique of measuring curvature. Alternatively the proposed method uses the same principle as in Eq. 1, but by measuring for the angle of incidence by the technique of magnetic induction. By measuring the directional tangents at the ends of the segments (represented by vectors $\mathbf{u}_1$ and $\mathbf{u}_2$ in $\mathbb{R}^3$), the angle of the arc length can be approximated, and the method can be extended for cumulatively reconstructing piecewise segments in 3D.

Let $\mathbf{p}_x(t)$ be a 3D vector, providing a parametric representation of the position of a particle moving through the x^{th} segment of the curve where $0^\circ \leq t \leq \theta_x$. The segments make up an overall piecewise curve, such that $\mathbf{p}_x(\theta_x) = \mathbf{p}_{x+1}(0^\circ)$, and the location of the first tangent $\mathbf{u}_{k=1}$ is placed at the origin, i.e. $\mathbf{p}_1(0^\circ) = 0$. As illustrated in Fig. 1b, to extend this technique to 3D, each pair of tangential vectors form an angle of incidence for each segment by the relationship of their dot products:

$$\theta_x = \cos^{-1}\left(\frac{\mathbf{u}_x \cdot \mathbf{u}_{x+1}}{|\mathbf{u}_x||\mathbf{u}_{x+1}|}\right) \tag{2}$$

More so, the plane at which the 3D curve is drawn along can be represented by its normal vector, $\mathbf{n}_x$, found by taking the cross-products of the pair of tangential vectors:

$$\mathbf{n}_x = \mathbf{u}_x \times \mathbf{u}_{x+1} \tag{3}$$

As seen in Figure 1b, by taking the cross product and assuming a uniform radius of curvature between each arc length, it can be illustrated that each segment is drawn as an arc of a great circle bisecting a sphere of radius r_x. From Eq. (3), the unit vector indicating the direction of the radius from the point at the beginning of each segment is given by:

$$\hat{\mathbf{r}}_x = \frac{\mathbf{n}_x \times \mathbf{u}_x}{|\mathbf{n}_x \times \mathbf{u}_x|} \tag{4}$$

By multiplying Eq. (4) with its scalar value found by Eq. (1) (i.e. $\mathbf{r}_x = r_x\hat{\mathbf{r}}_x$), the full vector for the radius of curvature is provided. Following this, the position of the center of curvature of the arc is calculated by simple vector addition:

$$\mathbf{c}_x = \mathbf{p}_x(0^\circ) + \mathbf{r}_x \tag{5}$$

Therefore, by obtaining the radius vector, the angle between vectors and the center of curvature, the x^{th} segment of the curve can be drawn out by:

$$\mathbf{p}_x(t) = |\mathbf{r}_x|(-\cos(t)\hat{\mathbf{r}}_x + \sin(t)\hat{\mathbf{u}}_x) + \mathbf{c}_x, \tag{6}$$

for $0^\circ \leq t \leq \theta_x$.

B. Magnetic Field Production and Sensing

Let the 3 orthogonal directions, X, Y, and Z, be generalised by i. Within the volume of interest, three magnetic fields, $B_i(t)$ are produced uniformly at separate frequencies, ω_i. Since the field strength of an electromagnetic coil is proportional to the current flowing through its windings, as illustrated in Fig. 2a. the magnetic field is generated by a voltage-controlled current source, such that the voltage reference, $V_{\text{ref},i} = \sin(\omega_i t)$, provides the sinusoidal reference frequency for each corresponding coil. A type of coil practical for this application are Helmholtz pairs, which have a uniformity within 2% accuracy, working within a normalised area of 0.4 times the radius [7].

Letting θ_X, θ_Y, and θ_Z be the angles between the sensor's axial vector and the three-coordinate axes unit vectors, **i**, **j** and **k**, the unit vector $\mathbf{u}_k$ which corresponds to the angular

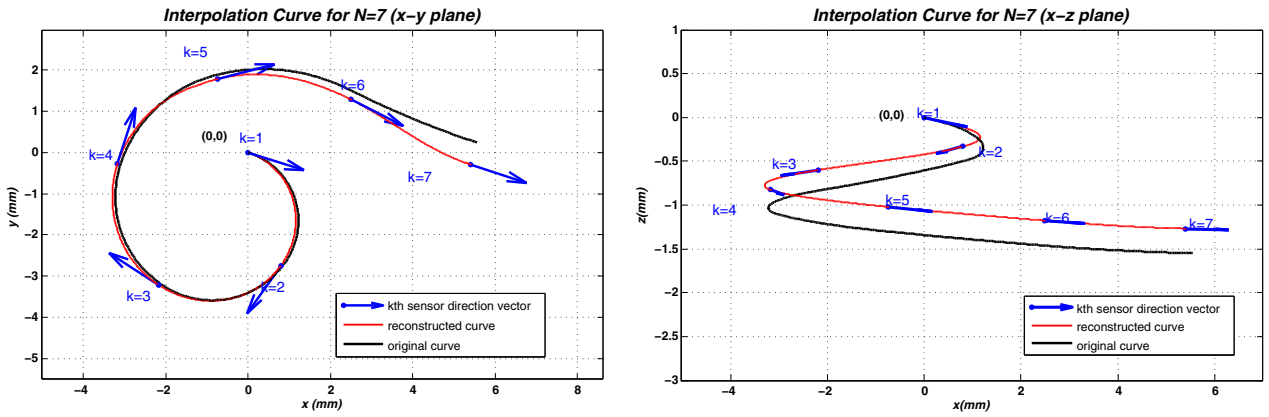

Fig. 3: Plot of 3D reconstructed array against controlled generated contour.

orientation of the k^{th} sensor of the array can be expressed in terms of its direction cosines:

$$\mathbf{u}_k = \cos(\theta_{X,k})\mathbf{i} + \cos(\theta_{Y,k})\mathbf{j} + \cos(\theta_{Z,k})\mathbf{k} \tag{7}$$

Each direction cosine can be measured by using axial magnetic coil sensors to sense fields in the directions of the three-axes unit vectors. By Faraday's law, the amplitude of electromotive force (emf) induced, $\varepsilon(t)$, is proportional to the direct cosine of the angle between the directions of the sensor's axis and the independent axes (i.e. $\varepsilon(t) \propto \cos\theta_i$).

The measured voltage response of the k^{th} sensor, $V_k(t)$, is an indirect measurement of the emf, since the sensor has a 2nd-order frequency response due to its parasitic capacitance from the closely wounded wire [8]. To measure and calculate the voltage response at targeted frequencies, a coupled Resistor-Capacitor tuning circuit is used.

C. Signal Processing

Measuring the voltage response in each sensor, gives a response in the format of:

$$\begin{aligned}\mathbf{V}_k(t,\theta_i) = {} & V_{0,X}\cos\theta_{X,k}\sin(\omega_X t + \Phi_{0,X}) \\ & + V_{0,Y}\cos\theta_{Y,k}\sin(\omega_Y t + \Phi_{0,Y}) \\ & + V_{0,Z}\cos\theta_{Z,k}\sin(\omega_Z t + \Phi_{0,Z})\end{aligned} \tag{8}$$

As shown in Fig. 2b, to extract the direct cosine dependence of each frequency, we use three single-phase phase-sensitive demodulators (PSDs) by multiplying the signal by the phase-shifted reference voltages ($V'_{\text{ref},i}$) (shifted by the known a priori constant phase responses, $\Phi_{0,i}$). Since the sine waves of differing frequencies are orthogonal, the product of its multiplication followed by a low-pass filter, yields a signed DC output signal proportional to the constant amplitude and cosine dependence.

$$V_k \times V'_{ref,i} => V_{\text{psd}(i,k)} = \frac{1}{2}V_{0,i}\cos\theta_{i,k} \tag{9}$$

The constant amplitude signal ($V'_{0,i} = \frac{1}{2}V_{0,i}$) can be removed if measured and configured beforehand, such that the direction cosine can be found by:

$$\mathbf{u}_k = \begin{bmatrix} V_{\text{psd}(X,k)}/V'_{0,X} \\ V_{\text{psd}(Y,k)}/V'_{0,Y} \\ V_{\text{psd}(Z,k)}/V'_{0,Z} \end{bmatrix} \tag{10}$$

III. Characterizing Accuracy

To test the accuracy of the method used for reconstruction, summarised in section II-A, a model of the path of a typical scala tympani chamber, generated by [9] was used to characterise a typical shape that an electrode array would settle in the scala tympani chamber. A 22.7mm segment of the path's basal curve length was taken to represent the path of a fully implanted electrode array. The curve was segmented into equidistant arc lengths, by parameterising the curve by length l, instead of angle t. The tangents and coordinates were extracted at each segment boundary (where the sensors' position would be situated) and used as inputs for the reconstruction method as described in Eqs. 1- 6 and implemented with MATLAB. The final points of the reconstructed curve were re-analysed to measure the accuracy of the position of the tangents by measuring the differences x, y and z coordinates from the set of given sensor points on the original curve. Fig. 3 demonstrates a graphical comparison of the original curve (black) with the reconstructed curve (red).

IV. Results and Discussion

The errors plotted in Fig. 4 are the inaccuracies of reconstructed positions of each k^{th} sensor, for N = 7, 9, 12, 16, 18 and 22. The error differences were presented in terms of the x-y deviation ($\text{error}_{xy} = \sqrt{\Delta x^2 + \Delta y^2}$) (left), to asses the efficacy of the technique in 2D, and the z-distance ($\text{error}_z = \Delta z$) (right), extending to 3-dimensions. For scalability, all lengths were normalised for the length of the electrode array. To analyse within the means of manufacturability, the error was characterised for the increase in the number, N, of equidistant sensors of up to 22. Fig. 4 expectedly demonstrates that increasing the resolution along the array by implementing a larger number of sensors contributes to a decrease in average error.

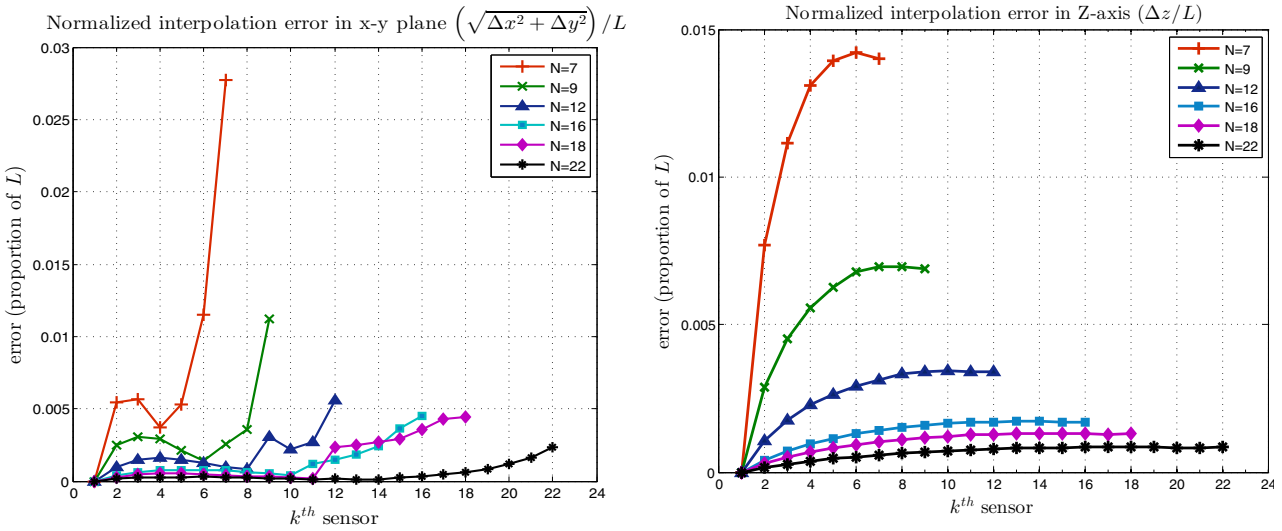

Fig. 4: Relative XY error (left) and relative Z error (right) normalized for the length of the electrode (22.7mm)

By inspecting both graphs, it can be seen that the error due to the reconstruction method had a worst-case error of less than 0.5% (relative to the length of the array) for 16 or more sensors along the array. This evaluation can also be used similarly to evaluate against the 2D method in [6], but for instead the implemented 9 strain gauge sensors.

However this analysis forms a characterization of error for only one curve at a typical constant shape. To account for the variations in irregular electrode array contours in instances that would indicate insertion faults such as buckling, tip fold-over or membrane perforation, the number of optimal electrodes would be greater than the minimum provided in this discussion to have higher resolution for more acute differences in tangent angles.

V. Conclusion and Future Work

Using this analysis, the number of coil sensors is selected in implementing a 10:1 scale model of the prototyped electrode array and external system, selecting the number of coil sensors for the given characterised worst-case error. The scaled model shown in Fig. 5, implements the design by sourcing orthogonal Helmholtz coils at frequencies of 85, 100 and 115kHz at magnetic field densities of no more than an estimated 6.36×10^{-5} Tesla. The signals are acquired digitally before performing the PSD, where the contour of the electrode array is visualised within MATLAB. Code division multiplexing could be used to provide more coils axis and reduce the influence of external noise at specific frequencies [10]. Using this implemented system, further feasibility testing will explore the external effects of noise and its scalability, while accounting for variations in the reconstruction method.

Fig. 5: Implementation of imaging system as a 10:1 scale proof of concept

References

[1] L. K. Holden, C. C. Finley, J. B. Firszt, T. A. Holden, C. Brenner, L. G. Potts, B. D. Gotter, S. S. Vanderhoof, K. Mispagel, G. Heydebrand *et al.*, "Factors affecting open-set word recognition in adults with cochlear implants," *Ear and Hearing*, vol. 34, no. 3, pp. 342–360, 2013.

[2] R. Shepherd, S. Hatsushika, and G. Clark, "Electrical stimulation of the auditory nerve: the effect of electrode position on neural excitation," *Hearing Research*, vol. 66, no. 1, pp. 108–120, 1993.

[3] E. Saunders, L. Cohen, A. Aschendorff, W. Shapiro, M. Knight, M. Stecker, B. Richter, S. Waltzman, M. Tykocinski, T. Roland, R. Laszig, and R. Cowan, "Threshold, comfortable level and impedance changes as a function of electrode-modiolar distance," *Ear and Hearing*, vol. 23, no. 1, pp. 28S–40S, 2002.

[4] M. Zrunek and K. Burian, "Risk of basilar membrane perforation by intracochlear electrodes," *Archives of oto-rhino-laryngology*, vol. 242, no. 3, pp. 295–299, 1985.

[5] A. J. Fishman and R. A. Holliday, "Principles of cochlear implant imaging," *Cochlear implants*, pp. 69–95, 2006.

[6] J. Wang and K. D. Wise, "A thin-film cochlear electrode array with integrated position sensing," *Microelectromechanical Systems, Journal of*, vol. 18, no. 2, pp. 385–395, 2009.

[7] E. L. Bronaugh, "Helmholtz coils for calibration of probes and sensors: limits of magnetic field accuracy and uniformity," in *Electromagnetic Compatibility, 1995. Symposium Record., 1995 IEEE International Symposium on*, pp. 72–76.

[8] P. Beiersdorfer and E. Clothiaux, "High-frequency magnetic measurements using small inductive probes," *Journal Name: Am. J. Phys.; (United States); Journal Volume: 51:11*, pp. Medium: X; Size: Pages: 1031–1036, 1983.

[9] J. R. Clark, F. M. Warren, and J. J. Abbott, "A scalable model for human scala-tympani phantoms," *Transactions of the ASME-W-Journal of Medical Devices*, vol. 5, no. 1, p. 014501, 2011.

[10] A. McEwan, J. Tapson, A. van Schaik, and D. S. Holder, "Code-division-multiplexed electrical impedance tomography spectroscopy," *Biomedical Circuits and Systems, IEEE Transactions on*, vol. 3, no. 5, pp. 332–338, 2009.